Empirical evidence for cosmogenic ³He production by muons 1 2 I.J. Larsen¹, K.A. Farley², M.P. Lamb², C.J. Pritchard³ 3 4 ¹Department of Geosciences, University of Massachusetts, Amherst, MA, USA; 5 ilarsen@umass.edu 6 7 ²Division of Geological and Planetary Sciences, California Institute of Technology, Pasadena, CA, USA 8 ³Department of Geology, Eastern Washington University, Cheney, WA, USA 9 10 **Abstract** 11 Cosmic ray muons penetrate deeply into rock where they interact with atoms to produce 12 cosmogenic nuclides. Incorporation of the muon contribution to the production rates of 13 cosmogenic nuclides increases the accuracy of exposure dates, burial ages, and erosion rates 14 inferred from measured nuclide concentrations. In the absence of empirical evidence, it is 15 generally assumed that muons do not produce ³He, a cosmogenic nuclide commonly used for 16 exposure dating. Here we assess whether muons produce ³He by measuring He isotope 17 18 concentrations in pyroxene and ilmenite from a ~300 m deep drill core and other subsurface samples of the mid-Miocene Columbia River Basalt in Washington, USA. ³He concentrations in 19 our samples exhibit an exponential decline with depth with an e-folding length of 32.4 m, which 20 corresponds to an attenuation length for ³He production of 8780 g cm⁻². The deeply penetrating 21 exponential is diagnostic of ³He production by cosmic ray muons. Assuming no erosion, we 22 constrain the minimum surface muonogenic production rate to be 0.23 atom g⁻¹ pyroxene yr⁻¹, 23

whereas when incorporating erosion the production rate is 0.45 atom g ⁻¹ pyroxene yr ⁻¹ . ³ He
concentrations in samples deeper than ~100 meters are consistent with model-based estimates of
depth-independent nucleogenic production from the capture by ⁶ Li of neutrons produced by
alpha particle reactions on light elements. Measurements in other subsurface samples indicate
that muon-produced ³ He is prevalent across the Columbia Plateau. The penetration depth of
muonogenic ³ He production is substantially deeper, and the ratio of muon- to spallation-
produced ³ He is substantially lower, than found for other cosmogenic nuclides. Our results
provide the first definitive empirical evidence for ³ He production by muons, which has several
implications for quantifying the timing and rates of Earth surface change and interpreting He
isotope ratios. Importantly, despite the low production rates, landforms in the Channeled
Scablands, which were formed by incision of the Columbia River Basalt by the late-Pleistocene
Missoula floods, have high concentrations of ³ He inherited from post-Miocene muon exposure.
Hence ³ He production by muons must be considered, particularly when dating rapid erosional
events in old bedrock. Our findings indicate samples with less than several tens of meters of
shielding by overlying rock will contain cosmogenic ³ He that elevates ³ He/ ⁴ He ratios. Hence
caution should be used when using ³ He/ ⁴ He ratios from samples at shallower depths to infer
mantle sources of basalt.

- **Keywords:** ³He; cosmogenic nuclides; muon; exposure dating; Columbia River Basalt;
- 43 Channeled Scablands, mantle helium

1. Introduction

The collision of galactic cosmic rays with atomic nuclei at the top of Earth's atmosphere generates a cascade of reactions that produce secondary cosmic rays. The secondary cosmic rays that reach Earth interact with atoms in rock to generate cosmogenic nuclides. At Earth's surface, cosmogenic nuclide production is dominated by spallation reactions induced by high energy nucleons, predominantly neutrons. In contrast, production at depths greater than a few meters is dominated by muons – subatomic particles with similar properties, but greater mass than electrons – which interact weakly with rock. For nuclides such as ¹⁰Be and ²⁶Al, muons are responsible for only ~2% of the total nuclide production at Earth's surface (Dunai, 2010). Hence for typical exposure dating and erosion rate applications of cosmogenic nuclides, errors introduced by uncertainty in nuclide production rates via muons are small relative to other sources of uncertainty (Balco, 2017). Accurately constraining nuclide production rates by muons is, however, very important for burial dating applications of cosmogenic nuclides because postburial nuclide production must be constrained (Granger and Muzikar, 2001; Balco, 2017). Additionally, cosmogenic nuclide-measured erosion rates in rapidly eroding landscapes are more accurate when production by muons is considered, because the ratio of muon- to nucleonproduced nuclides at the surface increases with erosion rate (Cerling and Craig, 1994; Balco et al., 2008). The ratio of nucleon versus muon nuclide production also varies with altitude (Lal, 1991), hence separate nucleon and muon production rate scaling relationships are required to compare exposure ages from sample suites that span a large range in elevation. Because there are a range of cosmogenic nuclide applications in which predictions are improved by constraining production rates from muons, there have been many efforts to quantify production rates for commonly-used nuclides, such as ¹⁰Be, ²⁶Al, ³⁶Cl, ²¹Ne, and ¹⁴C (Brown et al., 1995; Stone et al.,

46

47

48

49

50

51

52

53

54

55

56

57

58

59

60

61

62

63

64

65

66

1998; Braucher et al., 2003; Braucher et al., 2011; Braucher et al., 2013; Lupker et al., 2015;
Balco, 2017; Balco et al., 2019).

70

71

72

73

74

75

76

77

78

79

80

81

82

83

84

85

86

87

88

89

³He is a stable cosmogenic nuclide that is widely used for exposure dating (Cerling, 1990; Niedermann, 2002) and also has applications for determining erosion rates (Craig and Poreda, 1986; Gayer et al., 2008; Ferrier et al., 2013; Mackey et al., 2014) and in burial dating (Schiffer et al., 2020). Although theory suggests high energy muon and negative muon capture reactions both produce ³He (Lal, 1987; Nesterenok and Yakubovich, 2016), there is a lack of definitive empirical evidence for such production (Farley et al., 2006). Hence although production rate calibration datasets may implicitly include muon-produced ³He, separate scaling relationships for production by nucleons and from muons are not considered when calibrating ³He production rates (Goehring et al., 2010) or interpreting cosmogenic ³He concentrations (Balco et al., 2008; Marrero et al., 2016). However, some observations do suggest ³He is produced by muons. Measured ³He concentrations from a 10-meter depth-profile in a slowlyeroding landscape in Brazil are higher than predicted for production solely by energetic nucleons (Shuster et al., 2012). The high concentrations are consistent with production by muons, however, vertical mixing within the regolith offers an alternative explanation (Shuster et al., 2012). Higher ³He concentrations than expected from high energy nucleon production have also been measured in drill cores from Hawaii (Kurz, 1986a; Kurz et al., 1996). Muonogenic and nucleogenic ³He, which is produced by capture of non-cosmogenic neutrons by Li, ⁶Li(n, α)³H \rightarrow ³He, are both possible sources of ³He in the deep samples from Hawaii (Kurz, 1986a; Kurz et al., 1996). However, it is challenging to unambiguously distinguish between these two sources and hence isolate ³He production by muons.

To directly test whether ³He is produced by cosmic ray muons, we measured ³He in Miocene-age Columbia River Basalt samples in eastern Washington, USA collected to a depth of >300 m. The samples are from the Columbia Plateau, a dry, low-relief landscape that has undergone little erosion since the cessation of basalt eruptions and, with the exception of localized incision by the Pleistocene Missoula floods (Bretz, 1932), the original surface of the plateau has been largely preserved (Swanson and Wright, 1978). Old bedrock, low erosion rates, and constraints on nucleogenic ³He production (Larsen et al., 2019) make the Columbia Plateau an optimal setting to investigate whether ³He is produced by muons.

2. Study Area and Methods

Continental flood basalt volcanism in the mid-Miocene generated the 210,000 km³

Columbia River Basalt Group in the northwest U.S. (Reidel et al., 2013). Our samples come from two basalt units, the Wanapum and Grande Ronde Basalts. The Wanapum Basalt consists of ~68 individual flows (Reidel et al., 2013) that erupted from 16.2 to 15.9 Ma (Kasbohm and Schoene, 2018). The Grande Ronde Basalt, which makes up >70% of the Columbia River Basalt volume, began erupting after 16.6 Ma and the last eruption is dated to 16.1 Ma (Kasbohm and Schoene, 2018). The Wapshilla Ridge member, which is the oldest unit of the Grand Ronde basalt at our core site, erupted rapidly at 16.3 Ma (Kasbohm and Schoene, 2018). The average interval between the ~110 individual Grand Ronde Basalt flows is estimated to be only a few thousand years (Barry et al., 2010).

We measured ³He and ⁴He concentrations in pyroxene or ilmenite from 21 Columbia River Basalt samples from a core drilled in Cheney, Washington (Fig. 1). The core, from Cheney water well number 5, extends through the entire sequence of the Columbia River Basalt that was emplaced at Cheney. The Priest Rapids Member of the Wanapum Basalt extends from the surface of the core to a depth of 53 m (Reidel, 2005). The Priest Rapids Member was the last Columbia River Basalt member emplaced in the Cheney area (Reidel et al., 2013; Pritchard et al., 2020). The youngest Priest Rapids Member flow emplaced at Cheney is still preserved and field observations of vesiculated upper portions of the flow near the Cheney core site indicate there has been minimal erosion of the basalt surface. The remainder of the core to a depth of 335 m is Grande Ronde Basalt. Regional stratigraphy indicates the final eruptive member, the Sentinel Bluffs Member, is located at the top of the Grand Ronde Basalt and the lowermost basalt in the core is the Wapshilla Ridge Member (Pritchard et al., 2020). The depth of each sample with respect to the surface of the Columbia River Basalt was determined from the core log, and ranged from 3.9 to 303.9 m. Each sample was approximately 15 to 20 cm thick. The core log indicates the basalt was overlain by 1.8 m of soil and gravel, hence the uppermost sample was 5.7 m below the ground surface. The core samples were selected from areas >4m below the tops of individual basalt flows and unconformities to avoid sampling rock that may have been exposed to spallation by nucleons between successive flows. Here the term "spallation" refers to reactions initiated by the high energy cosmic ray protons and neutron flux in the uppermost few meters of rock, and explicitly excludes neutrons produced at greater depths by cosmogenic muon reactions. Additional samples of Wanapum and Grand Ronde Basalt were collected from sites that

113

114

115

116

117

118

119

120

121

122

123

124

125

126

127

128

129

130

131

132

133

134

135

Additional samples of Wanapum and Grand Ronde Basalt were collected from sites that were shielded from spallation reactions, including road-cut and quarry outcrops and from within small caves and columnar joint interstices. Six such samples were collected in a vertical traverse near Frenchman Coulee and additional samples were collected at Moses Coulee (n=5), Drumheller Channels (n=4) Potholes Coulee (n=1) and in and near Grand Coulee (n=3) (Fig. 1).

For samples collected from outcrops and roadcuts that were within 10 m of the surface, the depth below the original basalt surface was determined by surveying with a laser rangefinder. For samples >10 m below the uppermost basalt surface, the depth was determined by subtracting the sample elevation determined with a hand-held GPS from the elevation of the top of the basalt determined from aerial imagery and a 10-m horizontal resolution digital elevation model. The non-core samples were collected from depths of 3 to 158 m below the basalt surface. Due to the uncertainty associated with projecting the shielded samples to a common elevation with respect to the Miocene surface of the basalt, which has been eroded by the Missoula floods to varying degrees at each sample location, we do not use those data to quantify a muon production rate; rather we use them to qualitatively assess whether the results from the core are broadly valid across the Columbia Plateau.

The methods for generating pyroxene and ilmenite mineral separates for He measurement follow Larsen et al. (2019) and are summarized here. Samples were crushed and sieved to generate ~100 g of material in the 75-212 µm or 106-212 µm size fraction; we began separating the larger 106-212 µm size fraction after it was suggested that atmospheric ³He may adsorb to minerals with high specific surface areas (Protin et al., 2016), though we have not observed that this occurs for our samples. The crushed rock was leached for 24 h in hot, dilute HNO₃ and then underwent a series of multi-day leaches in solutions with progressively declining HF concentrations of 5% to 0.25% and 2% HNO₃ using a heated ultra-sonic bath. Once poly-mineral grains were disaggregated into single crystals, a lithium heteropolytungstate heavy liquid was used to separate pyroxene and ilmenite from plagioclase grains that were not fully dissolved by the acid leaching. Pyroxene and ilmenite grains were separated from each other with a Frantz isodynamic magnetic separator. ³He and ⁴He were measured at the Caltech Noble Gas Lab on

either a MAP 215-50 or a ThermoFisher Helix SFT noble gas mass spectrometer following heating to 1300°C under vacuum to release He, as described by Amidon and Farley (2011). Whole rock major oxide and trace element chemistry were measured by XRF following Litetraborate fusion of rock powders at Washington State University (Johnson et al., 1999).

Helium was measured in mineral separates from a total of 40 individual rock samples. Ten of those samples yielded both ilmenite and pyroxene and He was measured in both phases. Replicate He measurements were made for one sample (SCAB-095); hence there were a total of 51 He measurements, 24 of which were from the core (Table 1, Table S1). Because the production rate of ³He differs in ilmenite compared to pyroxene, to generate a dataset of comparable concentrations, we transformed all ³He concentrations in ilmenite to a pyroxene-equivalent value using the production ratio 0.78±0.02 (Larsen et al., 2019) and added uncertainties in quadrature. We omitted two ilmenite-pyroxene sample pairs (from 3.9 and 43.2 m depth) from the fitting routine described below because the measured ³He ratio in ilmenite to pyroxene was >1, which is considerably higher than the production ratio and indicates at least one of the measurements was anomalously high or low.

Knowledge of rock density is necessary to convert depth in meters to mass of overburden when assessing the penetration of muons into the crust. Specific gravity was measured for 26 samples from the Cheney core by weighing samples in air and while submerged in water.

Vesicular samples were wrapped in Parafilm® before being weighed in water and specific gravity values were corrected for Parafilm® specific gravity. The mean specific gravity was 2.81 for non-vesicular and 2.31 for vesicular samples, respectively. We used a weighted mean value of 2.71 g cm⁻³ value for rock density based on the relative proportions of non-vesicular and vesicular basalt observed in the core.

3. Results

Helium isotope ratios (³He/⁴He) in pyroxene and ilmenite separates are all substantially lower than the atmospheric ratio with higher ratios at shallower subsurface depths. ⁴He concentrations show no systematic variation with depth (Table 1). In contrast, ³He concentrations in the Cheney core exhibit a clear exponential decline with depth for depths <100 m (Fig. 2). At greater depths, the ³He concentrations are largely depth-invariant and are a small fraction of the values higher in the core. The ³He concentration-depth relationship for the non-core samples collected from sites shielded from production by nucleons conform to the trend apparent in the core (Table S1), with concentrations that decline exponentially at depths less than ~100 m, but become invariant at great depth (Fig. 2). The deeply penetrating exponential trend in ³He concentrations is consistent with production by muons. Below, we use the depth profile to define the production of muonogenic ³He as a function of depth, as has been done for other muon-produced cosmogenic nuclides (Braucher et al., 2013) or for spallation-produced ³He in shallow cores (Farley et al., 2006).

4. Analysis: Attenuation length and production rates

We interpret ³He in our samples to have been produced by two fundamentally different processes. Nucleogenic ³He is generated by capture on ⁶Li of neutrons arising from interaction of alpha particles with light elements (Andrews and Kay, 1982). Nucleogenic ³He production thus depends on chemistry, but not on subsurface depth. Cosmogenic ³He is traceable to cosmic ray irradiation, and is produced by three different reactions involving: a) spallation by high energy neutrons and protons, b) neutrons produced by high energy nucleons which then thermalize and

are captured by ⁶Li (Dunai et al., 2007), and c) muons. Mantle ³He is another component we have considered, but because the crystals we fuse to release He are very small, any fluid inclusions that may contain mantle He would also be small. Hence we explicitly assume no mantle ³He (Larsen et al., 2019). Even if our small grains were to have as much mantle ³He as reported by Dodson et al. (1997) for >400 um olivine grains from a Wanapum basalt flow (0.09x10⁶ atom g⁻¹), it would account for only a few percent of the ³He measured in the upper core samples and 16% of what we measured in the core sample with the lowest ³He concentration. Because the production of ³He from cosmogenic thermal neutrons is a small fraction of the spallation production, and has a similar depth dependence, it is common practice to combine the two into a single term. We adopt that practice here.

At any given depth z, the total production rate of ${}^{3}\text{He }P$ is:

$$P(z) = P_{s0}e^{\left(-\frac{z\rho}{\Lambda_s}\right)} + P_{m0}e^{\left(-\frac{z\rho}{\Lambda_m}\right)} + P_{nuc}$$
 (1)

where the subscripts s, m, and nuc refer to spallogenic, muonogenic, and nucleogenic production, respectively and the subscript 0 refers to production at the Earth's surface. Here we assume that nucleogenic 3 He production is invariant with depth because Columbia River Basalt chemistry is fairly uniform (Hooper, 2000), which is confirmed by the whole rock chemistry of our core samples (Table S2). Similarly, we use a constant rock density ρ of 2.71 g cm⁻³ as described above. The spallation component has a characteristic attenuation length Λ_s that we take to be 160 g cm⁻², based on prior work (Dunai, 2010); coupled with density this value implies an e-folding length of 59 cm for spallation production. The surface spallation production rate P_{s0} in the phases we analyzed is also known from altitude-latitude scaling relationships based on

geological calibration data (Goehring et al., 2010; Marrero et al., 2016; Larsen et al., 2019). The muonogenic 3 He production attenuation length Λ_{m} , the surface production rate P_{m0} , and P_{nuc} are unknowns that we seek to determine from our depth profile.

In a given geologic situation, each of the three production mechanisms in equation (1) will operate over a potentially distinct duration to produce the measured concentration profile. For example, in a basalt, the nucleogenic component will accumulate throughout the lifetime of the rock. In contrast, the spallation and muonogenic components will accumulate only when the rock is sufficiently close to the surface to receive high energy nucleons and muons, respectively. In the Cheney core and most of our other samples, the shielding is sufficient to essentially eliminate production by spallation. For example, the uppermost core sample used in our fitting routine comes from 610 cm below the basalt surface. At this depth the spallation production is reduced to ~30 ppm of the surface value. Thus at this depth and deeper, the first term in equation (1) is negligible and we assume it is equal to zero. In the case of no production via spallation, the depth dependence of a ³He concentration depth profile developed by muon and nucleogenic reactions can be described by:

$$N(z) = N_{m0}e^{\left(-\frac{z\rho}{\Lambda_m}\right)} + N_{nuc}$$
 (2)

where N is nuclide concentration, which allows for a robust determination of the unknown parameters N_{m0} , Λ_m , and N_{nuc} by fitting equation (2) to data.

We estimated initial values of N_{m0} and N_{nuc} by iteratively fitting equation (2) using linear least squares regression applied to depth z on the x-axis and $\ln(N(z) - N_{nuc})$ on the y-axis, and evaluated the correlation coefficient (\mathbb{R}^2). We began by fitting all samples from depths

<250 m and repeated the fit after successively removing the deepest samples below an arbitrary cutoff depth. We calculated the mean 3 He concentration in all samples below the cutoff depth for inclusion in the best fit to equation (2) and assumed this value equals N_{nuc} . We determined the best model fit by finding the cutoff depth that produced the highest R^2 value. The best fit was achieved for a N_{nuc} value of 0.71 x10⁵ atom g^{-1} , which was based on the mean 3 He concentration in all samples with depths > 87 m. The best fit N_{m0} was 5.1x10⁶ atom g^{-1} and the best fit value of the e-folding length was 32.4 m, which corresponds to an Λ_m of 8780 g cm⁻² for a rock density of 2.71 g cm⁻³. The residuals are evenly distributed about zero and show no trends (Fig. 3), indicating equation (2) is an appropriate model for our data.

There are two endmember scenarios for calculating the surface muonogenic 3 He production rate. Assuming no erosion and constant accumulation of muon produced 3 He since the time of basalt eruption t, we calculate P_{m0} as:

$$P_{m0} = N_{m0}/t (3)$$

and using t = 15.9 Ma, the age for the latest Wanapum Basalt eruption (Kasbohm and Schoene, 2018), equation (3) yields a local surface muon production rate of 0.32 atom g^{-1} yr⁻¹. Based on the muonogenic scaling methods of Stone (2000), the production rate scaled to sea level is 0.23 atom g^{-1} yr⁻¹. This production rate is effectively an average over the ~16 Ma lifetime of the basalt and is a firm lower limit because erosion can only shorten the exposure duration.

Alternatively, assuming steady erosion of the basalt over the lifetime of the basalt (t = 15.9 Ma), the surface muon concentration can be determined from (Lal, 1991; Niedermann, 2002; Dunai, 2010):

$$N_{m0} = \frac{P_{m0}}{\rho \varepsilon / \Lambda_m} e^{-\rho (z_0 - \varepsilon t) / \Lambda_m} \left(1 - e^{-(\rho \varepsilon / \Lambda_m)t} \right) \tag{4}$$

where ε is the erosion rate (cm yr⁻¹) that can be constrained from spallogenic ³He. The uppermost section of the Cheney core, which includes the top of the basalt, was not preserved. Hence we estimated a regional erosion rate of the plateau surface using the spallogenic ³He concentration in a sample (sample SCAB-015 in Fig. 1) collected from the uppermost basalt surface in an area lacking evidence of bedrock erosion by the Missoula floods (Bretz, 1932). The pyroxene-equivalent ³He concentration in the sample (Table S3) yields an erosion rate of 1.46±0.03 m Ma⁻¹, calculated using version 3 of the original CRONUS calculator of Balco et al. (2008). Solving equation (4) for P_{m0} yields a production rate of 0.45 atom g⁻¹ yr⁻¹. Scaled to sea level this corresponds to 0.32 atom g⁻¹ yr⁻¹. Note that the spallogenic ³He concentration constrains the erosion rate for only the last several hundred thousand years, yet our analysis assumes this value pertained throughout the 15.9 Ma lifetime of the Wanapum Basalt.

5. Discussion

The predicted spallation production rate of ³He in pyroxene at the core site, based on modified Lal (1991) 'Lm' scaling (Balco et al., 2008), is 228 atom g⁻¹ yr⁻¹ (Marrero et al., 2016). Hence the muonogenic ³He production rates we predict are only ~0.1% of that for spallation. The contribution of muons to the total surface production is approximately 2-3% for other cosmogenic nuclides (Balco, 2017), and theory predicts a similar contribution for ³He (Lal, 1987; Nesterenok and Yakubovich, 2016). Both shielding of the basalt surface by Quaternary deposits

and loss of nuclides by unsteady erosion of the basalt potentially result in underestimation of muonogenic production rates for our samples. For example, in the (unrealistic) limiting case of instantaneous erosion of ~100 meters from the surface of the core at 0.4 Ma (the exposure age implied by spallogenic ³He as described above) followed by no further erosion, the muonogenic production rate according to equation (3) would be ~13 atoms g⁻¹ yr⁻¹.

The Cheney core site was loess-covered prior to the Missoula floods. The drill log indicates the basalt at the core site was overlain by 1.8 m of soil and gravel, deposited during the megfloods that sculpted the loess at the site (Fig. 1). However, because the loess is young relative to the Columbia River Basalt (Busacca. 1989), shielding by Quaternary surficial deposits would only minimally reduce muonogenic ³He production at the basalt surface.

Erosion of the uppermost basalt by the Missoula floods could influence our inferred values of N_{m0} . The Cheney core sits at the margin of the Cheney-Palouse scabland tract, which was one of the paths taken by Missoula floods as they crossed the Columbia Plateau. There is no obvious evidence that basalt at the core site was scoured by Missoula floods, unlike the main Cheney-Palouse floodway, which contains coulee, butte, and basin topography carved into the basalt. Further, sensitivity analysis to assess how truncation of the basalt surface would influence our findings indicates that loss of the upper 5 m of the basalt would increase N_{m0} by only 15% (Fig. 4). We therefore infer that our muonogenic 3 He production rates are unlikely to be greatly influenced by an episode of erosion caused by outburst floods.

If the erosion rate at the core site was higher than at the location of sample SCAB-015 the inferred muonogenic ³He production rate would be proportionally higher. Sample SCAB-015 and the top of the Cheney core are from the same basalt member and are located at similar latitude on the generally flat, northern portion of the Columbia Plateau. Due to the similar

mineralogy, climatic, and geomorphic setting, we do not expect erosion rates to differ significantly between the two sites. Assuming erosion rates integrate over the timescale required to erode through a bedrock thickness equivalent to one e-folding length, the spallation-derived erosion rates average over a relatively long period of ~400 ka, because the erosion rate is very low. We know of no estimates of erosion rates on the Columbia Plateau that extend beyond the Quaternary time period, and if long-term erosion rate were higher, the muonogenic production rate would be greater than our estimated value.

The shielded samples we collected from sites scattered across the western part of the Columbia Plateau exhibit a deeply penetrating exponential concentration-depth relationship similar to what we observed in the Cheney core. For a given depth, some of the concentrations in the shielded samples are slightly higher than concentrations in the core samples, potentially due to over-estimation of the paleo-sample depth at some locations. The similar concentration-depth relation implies that the erosion rate at all of the sample locations has been about the same. The observation that the original surface of the Columbia plateau has been largely preserved since the Miocene (Swanson and Wright, 1978) and the presence of vesiculated flow tops near Cheney indicate that, except during late Pleistocene floods, post-Miocene erosion has been limited. Therefore, geological observations are consistent with our estimates of low erosion rates; and given the results from our shielded samples it is plausible that the surface of the Columbia River Basalt has been minimally stripped across most of the plateau.

The attenuation length of 8780 cm⁻² we obtained for muonogenic ³He production is roughly twice that determined and predicted for other cosmogenic nuclides (Heisinger et al., 2002; Braucher et al., 2013; Balco, 2017). The longer attenuation length cannot be attributed to uncertainties in the geologic history of the Columbia River Basalt as erosion only affects the

estimated surface production rate, not the depth dependence of cosmogenic production. Muons lose energy as they pass through rock. The simplest explanation for the observed production of muonogenic ³He at greater depths than nuclides like ¹⁰Be and ²⁶Al is that the threshold muon energy for ³He production is lower. We are unaware of any direct measurements of ³He production from muons comparable to those reported for cosmogenic radionuclides by Heisinger et al. (2002) by which to assess this hypothesis.

The near-constant, background ³He concentration in samples >87 m deep is indicative of nucleogenic production (Farley et al., 2006; Amidon et al., 2009). The background value of 0.71±0.13x10⁶ atoms g⁻¹ determined for the core samples is within 2σ uncertainty of the 0.37 to 0.54x10⁶ atom g⁻¹ range predicted from Li measurements in pyroxene and whole rock chemistry of Columbia River Basalt samples by Larsen et al. (2019) using the model of Amidon et al. (2008), which simulates neutron production, redistribution, and stopping rate on Li within host minerals. Hence our findings show the nucleogenic contributions to ³He production are well predicted by the Amidon et al. (2008) model and validate its predications of this non-cosmogenic ³He component.

Our finding that ³He is produced by muons is particularly important for accurately determining exposure ages in landscapes formed by rapid, recent incision of old rocks. Rapid erosion of tens of meters of rock may produce landforms that, at their inception, have large nuclide concentrations inherited from muonogenic production (Stone et al., 1998; Briner et al., 2016). Such a scenario might be relatively common in well fractured rock, like basalt, where erosion from large floods can be extremely rapid (e.g., Lamb and Fonstad, 2010; Lamb et al., 2014). The likelihood of incorrectly inferring exposure ages due to inheritance is greatest when the duration of exposure to muons was long, the landform is young, and exhumation was shallow

(Stone et al., 1998). The potential for inherited muon-produced nuclides to cause exposure dating errors in such settings is greatest for stable nuclides, such as ³He. Similarly, assessing the time interval between successive volcanic eruptions by exposure dating the tops of buried lava flows using ³He may be confounded by muonogenic production, especially in settings where the ratio of eruption age to inter-eruption time interval is high.

Dating Columbia Plateau erosional bedrock landforms created by the Missoula floods is a prime example of an application where knowledge of ³He production by muons at depth is essential. The ³He concentration-depth trend in the shielded samples we collected are consistent with the data from the Cheney core, indicating muon-produced ³He is present at depth across the Columbia Plateau. Comparison of the ³He concentrations from shielded samples with ³He measurements in both ilmenite and pyroxene against values in samples collected from Missoula flood-eroded surfaces published by Larsen et al. (2019), indicates many of the surface-exposed samples have a substantial component of inherited ³He from pre-Pleistocene muon exposure (Fig. 5). The four most deeply shielded samples collected >35 m below the pre-flood plateau surface have ³He concentrations distinctly lower than the surface samples of flood-eroded bedrock. However, the shielded samples from depths <10 m typically have high ³He concentrations that are comparable to many of the samples of the unshielded flood-eroded bedrock and flood-transported boulders. Hence correctly interpreting the measured concentrations as post-Pleistocene exposure ages demands correction for ³He accumulated during post-Miocene muon exposure.

Despite having variable proportions of spallation- and muon-produced ³He, both shielded and unshielded samples plot on a line that defines an ilmenite-to-pyroxene production ratio of 0.78 (Fig. 5). The production ratio is hence the same for muonogenic and spallogenic ³He

production in these two mineral phases, indicating muonogenic ³He in either mineral can be used to for dating or erosion rate measurements. The finding that the production ratio is the same also indicates our method of converting ³He concentrations in ilmenite to pyroxene-equivalent values for determining muonogenic production rates is valid.

Many studies measure ³He in a shielded sample and subtract the measured concentrations from surface samples prior to calculating exposure ages or erosion rates in order to correct for non-spallogenic ³He, but the shielded samples often are not collected at the same depth as the exposed sample (Marchetti and Cerling, 2005; Gayer et al., 2004; Amidon and Farley, 2011; Ferrier et al., 2013; Mackey et al., 2014). Due to production by muons, the concentration of ³He in a shielded sample will vary as a function of depth. In order to most accurately correct for ³He inherited from muon production, shielded samples should be collected from the same paleodepth as the samples that are to be dated. Alternatively, the muon penetration length and a single measured shielded sample can be used to predict the muonogenic ³He at any depth. Ice and water transported boulders are very common targets for exposure dating, but unless boulder provenance with respect to their depth below the land surface can be constrained, obtaining accurate exposure dates on boulders is unlikely in settings with high concentrations of muon-produced ³He. Likewise, using shielded samples to constrain non-nucleonic ³He concentrations when determining erosion rates in landscapes with considerable relief is likely to be complicated by the depth-dependence of muonogenic ³He concentrations.

The greater attenuation length for muonogenic production of cosmogenic nuclides allows erosion rates to be quantified over longer timescales than possible with spallation-produced nuclides (Braucher et al., 2003). Our findings indicate the attenuation length, and therefore the averaging time of erosion rate measurements, for ³He production by muons is about 20 times

greater than for spallogenic production. Profiles of muon-produced ³He can be used to extend the timescale of erosion rate measurements in landscapes with mafic bedrock by more than an order of magnitude, filling a methodological gap by providing a technique that averages over timescales between spallation-produced ³He and low-temperature thermochronology.

Burial dating requires an accurate determination of production rates by muons because post-burial nuclide production must be subtracted from measured concentrations to obtain burial ages (Balco, 2017). A ⁵³Mn/³He burial dating system is currently under development, where nuclide measurements in Fe-Ti oxides have potential to extend the range of burial dating to 25 Ma (Schiffer et al., 2020). Our findings indicate that muonogenic production must be accounted for in burial dating that utilizes ³He, especially when targeting old sediment for dating. The attenuation length and production rate values we have calculated provide a means for making the necessary corrections for post-burial nuclide production.

³He/⁴He ratios are commonly used to diagnose mantle sources of basalt (Class and Goldstein, 2005). Even very small amounts of cosmogenic ³He can influence inferred ³He/⁴He ratios (Kurz, 1986b). Collecting samples at few meter depths shielded from spallation-produced ³He is a common method to avoid inclusion of cosmogenic ³He when studying mantle sources (e.g., Dodson et al., 1997). However, the muonogenic ³He production demonstrated here indicates that several tens of meters of shielding are required to fully preclude cosmogenic ³He. To analytically discriminate between mantle and other ³He sources, samples are typically crushed under vacuum to release mantle He from inclusions, whereas high temperature fusion is used to release matrix-hosted cosmogenic and radiogenic He (Kurz, 1986b). Energetic spallation reactions cause ³He and ³H to be redistributed within basalt with stopping ranges that can exceed 1 mm (Larsen et al., 2019). The same long range may also occur with muonogenic ³He

production. Such redistribution may implant ³He produced in rock into adjacent inclusions and may elevate the ³He/⁴He ratio measured by crushing. In addition, radiogenic ⁴He produced mostly in the rock matrix is typically stopped in about 15 microns. Thus there is likely to be physical separation of cosmogenic and radiogenic gases implanted in coarse-grained minerals like olivine and pyroxene used for mantle He studies. If so, fusion analyses revealing ³He/⁴He ratios lower than in the crush may be inadequate to prove the absence of cosmogenic addition to a crush analysis. These possibilities suggest caution in the interpretation of crush-released He in samples shielded by less than a few tens of meters.

6. Conclusions

Concentrations of ³He in ilmenite and pyroxene that extend from the surface through the entire sequence of the Columbia River Basalt exhibit an exponential decline with depth to 87m, which we attribute to cosmogenic ³He production by muons. We estimate that the attenuation length for ³He production by muons is 8780 g cm⁻² and the *e*-folding length is 32.4 m. The surface mounogenic production rate is 0.23 atom g⁻¹ pyroxene yr⁻¹ assuming no erosion; using spallation-produced ³He to constrain the erosion rate yields a muonogenic production rate of 0.45 atom g⁻¹ pyroxene yr⁻¹. ³He concentrations at depths >100 m are largely depth-invariant and the concentrations are well-predicted by a model for nucleogenic production. Our results provide the first definitive empirical evidence for ³He production by muons, which has important implications and applications for exposure dating, burial dating, and quantifying long-term erosion rates over 10⁵– to 10⁷–year timescales. Accounting for ³He production by muons is especially important in landscapes incised into old rock with a long-duration of exposure to

458 muons because recently eroded landforms will likely have significant inherited ³He from muon 459 production. 460 Acknowledgements 461 We thank Karin Lehnigk, Scott David, and Madison Douglas for assistance in the field, Devon 462 Dunajski, Patrick Scordato, and Alice Hough for helping separate minerals, Johnathan Treffkorn 463 464 for assistance with ³He measurements, and Stephen Riedel and Graysen Bjork for helpful 465 information pertaining to the Cheney core. We thank Marissa Tremblay for a constructive review. This research was supported by a collaborative NSF award (1529528, 1529110) to I.J.L., 466 467 K.A.F. and M.P.L. 468 References 469 Amidon, W. H. and Farley, K. A., 2011. Cosmogenic ³He production rates in apatite, zircon and 470 pyroxene inferred from Bonneville flood erosional surfaces. Quaternary Geochronology 6, 10-471 21. 472 Amidon, W. H., Farley, K. A., Burbank, D. W., Pratt-Sitaula, B., 2008. Anomalous cosmogenic 473 ³He production and elevation scaling in the high Himalaya. Earth and Planetary Science Letters 474 265, 287-301. 475 Amidon, W. H., Rood, D. H., Farley, K. A., 2009. Cosmogenic ³He and ²¹Ne production rates 476 calibrated against ¹⁰Be in minerals from the Coso volcanic field. Earth and Planetary Science 477

478

Letters 280, 194-204.

- Andrews, J. N. and Kay, R., 1982. Natural production of tritium in permeable rocks. Nature 298,
- 480 361-363.
- 481 Balco, G., 2017. Production rate calculations for cosmic-ray-muon-produced ¹⁰Be and ²⁶Al
- benchmarked against geological calibration data. Quaternary Geochronology 39, 150-173.
- Balco, G., Stone, J. O., Lifton, N. A., Dunai, T. J., 2008. A complete and easily accessible means
- of calculating surface exposure ages or erosion rates from ¹⁰Be and ²⁶Al measurements.
- 485 Quaternary Geochronology 3, 174-195.
- 486 Balco, G., Blard, P., Shuster, D. L., Stone, J. O., Zimmermann, L., 2019. Cosmogenic and
- nucleogenic ²¹Ne in quartz in a 28-meter sandstone core from the McMurdo Dry Valleys,
- 488 Antarctica. Quaternary Geochronology 52, 63-76.
- Barry, T. L., Self, S., Kelley, S. P., Reidel, S., Hooper, P., Widdowson, M., 2010. New ⁴⁰Ar/³⁹Ar
- dating of the Grande Ronde lavas, Columbia River Basalts, USA: Implications for duration of
- flood basalt eruption episodes. Litho. 118, 213-222.
- 492 Braucher, R., Bourlès, D., Merchel, S., Romani, J. V., Fernadez-Mosquera, D., Marti, K.,
- Leanni, L., Chauvet, F., Arnold, M., Aumaître, G., 2013. Determination of muon attenuation
- lengths in depth profiles from in situ produced cosmogenic nuclides. Nuclear Instruments and
- Methods in Physics Research Section B: Beam Interactions with Materials and Atoms 294, 484-
- 496 490.

- Braucher, R., Brown, E. T., Bourlès, D. L., Colin, F., 2003. In situ produced ¹⁰Be measurements
- 498 at great depths: implications for production rates by fast muons. Earth and Planetary Science
- 499 Letters 211, 251-258.
- Braucher, R., Merchel, S., Borgomano, J., Bourlès, D. L., 2011. Production of cosmogenic
- radionuclides at great depth: a multi element approach. Earth and Planetary Science Letters 309,
- 502 1-9.
- Bretz, J.H., 1932. The Grand Coulee. American Geographical Society, Special publication 15,
- 504 New York, 89 p.
- Briner, J. P., Goehring, B. M., Mangerud, J., Svendsen, J. I., 2016. The deep accumulation of
- ¹⁰Be at Utsira, southwestern Norway: implications for cosmogenic nuclide exposure dating in
- peripheral ice sheet landscapes. Geophysical Research Letters 43, 9121-9129.
- Brown, E. T., Bourlès, D. L., Colin, F., Raisbeck, G. M., Yiou, F., Desgarceaux, S., 1995.
- 509 Evidence for muon-induced production of ¹⁰Be in near-surface rocks from the Congo.
- 510 Geophysical Research Letters 22, 703-706.
- Burns, E. R., Morgan, D. S., Rachael, S. P., Rachael, S., Kahle, S. C., 2011. Three-Dimensional
- Model of the Geologic Framework for the Columbia Plateau Regional Aquifer System, Idaho,
- Oregon, and Washington. U.S. Geological Survey Scientific Investigations Report 2010-5246,
- 514 44 p.
- Busacca, A. J., 1989. Long Quaternary record in eastern Washington, USA, interpreted from
- multiple buried paleosols in loess. Geoderma 45, 105-122.

- 517 Cerling, T. E., 1990. Dating geomorphologic surfaces using cosmogenic ³He. Quaternary
- 518 Research 33, 148-156.
- 519 Cerling, T. E. and Craig, H. S., 1994. Geomorphology and in-situ cosmogenic isotopes. Annual
- Review of Earth and Planetary Sciences 22, 273-317.
- 521 Class, C. and Goldstein, S.L. 2005. Evolution of helium isotopes in the Earth's mantle. Nature
- 522 436, 1107-1110.
- 523 Craig, H. and Poreda, R. J., 1986. Cosmogenic He in terrestrial rocks: The summit lavas of Maui.
- Proceedings of the National Academy of Sciences 83, 1970-1974.
- Dodson A., Kennedy B. M. and DePaolo D. J. (1997) Helium and neon isotopes in the Imnaha
- Basalt, Columbia River Basalt Group: evidence for a Yellowstone plume source. Earth and
- 527 Planetary Science Letters 150, 443–451.
- 528 Dunai, T.J., 2010. Cosmogenic nuclides: principles, concepts and applications in the earth
- surface sciences. Cambridge University Press, 187 p.
- Dunai, T. J., Stuart, F. M., Pik, R., Burnard, P., Gayer, E., 2007. Production of ³He in crustal
- rocks by cosmogenic thermal neutrons. Earth and Planetary Science Letters 258, 228-236.
- Farley, K. A., Libarkin, J., Mukhopadhyay, S., Amidon, W., 2006. Cosmogenic and nucleogenic
- ³He in apatite, titanite, and zircon. Earth and Planetary Science Letters 248, 451-461.
- Ferrier, K. L., Perron, J. T., Mukhopadhyay, S., Rosener, M., Stock, J. D., Huppert, K. L.,
- Slosberg, M., 2013. Covariation of climate and long-term erosion rates across a steep rainfall

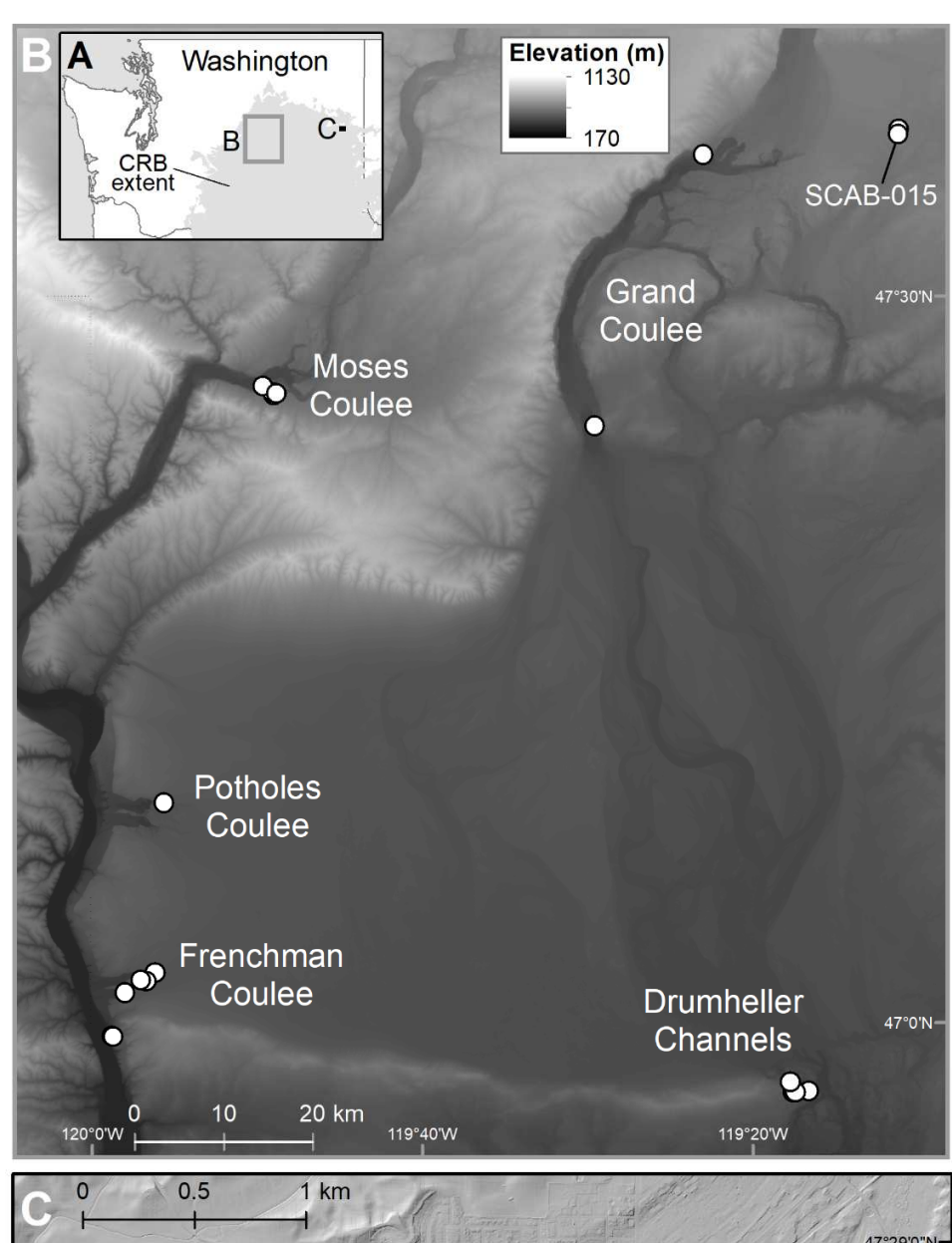
- gradient on the Hawaiian island of Kaua'i. Geological Society of America Bulletin 125, 1146-
- 537 1163.
- Gayer, E., Pik, R., Lavé, J., France-Lanord, C., Bourles, D., Marty, B., 2004. Cosmogenic ³He in
- Himalayan garnets indicating an altitude dependence of the ³He/¹⁰Be production ratio. Earth and
- 540 Planetary Science Letters 229, 91-104.
- Gayer, E., Mukhopadhyay, S., Meade, B. J., 2008. Spatial variability of erosion rates inferred
- from the frequency distribution of cosmogenic ³He in olivines from Hawaiian river sediments.
- Earth and Planetary Science Letters 266, 303-315.
- Goehring, B. M., Kurz, M. D., Balco, G., Schaefer, J. M., Licciardi, J., Lifton, N., 2010. A
- reevaluation of in situ cosmogenic ³He production rates. Quaternary Geochronology 5, 410-418.
- Granger, D. E. and Muzikar, P. F., 2001. Dating sediment burial with in situ-produced
- cosmogenic nuclides: theory, techniques, and limitations. Earth and Planetary Science Letters
- 548 188, 269-281.
- Heisinger, B., Lal, D., Jull, A. T., Kubik, P., Ivy-Ochs, S., Knie, K., Nolte, E., 2002. Production
- of selected cosmogenic radionuclides by muons: 2. Capture of negative muons. Earth and
- Planetary Science Letters 200, 357-369.
- Hooper, P. R., 2000. Chemical discrimination of Columbia River basalt flows. Geochemistry,
- 553 Geophysics, Geosystems. 1, 1024, doi:10.1029/2000GC000040.

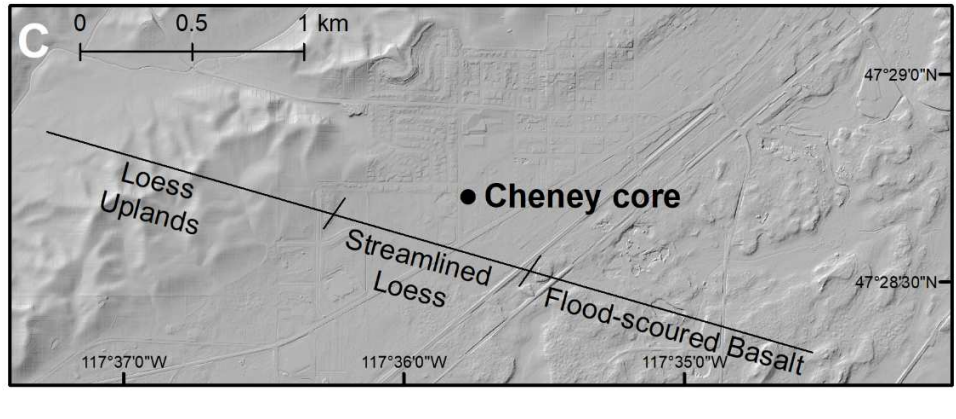
- Johnson, D. M., Hooper, P. R. and Conrey, R. M., 1999. XRF Analysis of rocks and minerals for
- 555 major and trace elements on a single low dilution Li-tetraborate fused bead. Advances in X-ray
- 556 analysis, 41, 843-867.
- Kasbohm, J. and Schoene, B., 2018. Rapid eruption of the Columbia River flood basalt and
- correlation with the mid-Miocene climate optimum. Science Advances 4, eaat8223.
- Kurz, M. D., 1986a. In situ production of terrestrial cosmogenic helium and some applications to
- geochronology. Geochimica et Cosmochimica Acta 50, 2855-2862.
- Kurz, M. D. 1986b. Cosmogenic helium in a terrestrial igneous rock. Nature 320, 435-439.
- Kurz, M. D., Kenna, T. C., Lassiter, J. C., DePaolo, D. J., 1996. Helium isotopic evolution of
- Mauna Kea Volcano: First results from the 1-km drill core. Journal of Geophysical Research:
- 564 Solid Earth 101, 11781-11791.
- Lal, D., 1987. Production of ³He in terrestrial rocks. Chemical Geology 66, 89-98.
- Lal, D., 1991. Cosmic ray labeling of erosion surfaces: in situ nuclide production rates and
- erosion models. Earth and Planetary Science Letters 104, 424-439.
- Lamb M. P., and Fonstad M. A. 2010. Rapid formation of a modern bedrock canyon by a single
- flood event. Nature Geoscience 3, 477-81.
- Lamb, M. P., Mackey, B. H., Farley, K. A., 2014. Amphitheater-headed canyons formed by
- 571 megaflooding at Malad Gorge, Idaho. Proceedings of the National Academy of Sciences 111, 57-
- 572 62.

- Larsen, I. J., Farley, K. A., Lamb, M. P., 2019. Cosmogenic ³He production rate in ilmenite and
- 574 the redistribution of spallation ³He in fine-grained minerals. Geochimica et Cosmochimica Acta
- 575 265, 19-31.
- Lupker, M., Hippe, K., Wacker, L., Kober, F., Maden, C., Braucher, R., Bourles, D., Romani, J.
- 577 V., Wieler, R., 2015. Depth-dependence of the production rate of in situ ¹⁴C in quartz from the
- Leymon High core, Spain. Quaternary Geochronology 28, 80-87.
- Mackey, B. H., Scheingross, J. S., Lamb, M. P., Farley, K. A., 2014. Knickpoint formation, rapid
- propagation, and landscape response following coastal cliff retreat at the last interglacial sea-
- level highstand: Kaua'i, Hawai'i. Geological Society of America Bulletin 126, 925-942.
- Marchetti, D. W. and Cerling, T. E., 2005. Cosmogenic ³He exposure ages of Pleistocene debris
- flows and desert pavements in Capitol Reef National Park, Utah. Geomorphology 67, 423-435.
- Marrero, S. M., Phillips, F. M., Borchers, B., Lifton, N., Aumer, R., Balco, G., 2016.
- Cosmogenic nuclide systematics and the CRONUScalc program. Quaternary Geochronology 31,
- 586 160-187.
- Nesterenok, A. V. and Yakubovich, O. V., 2016. Production of ³He in rocks by reactions induced
- by particles of the nuclear-active and muon components of cosmic rays: Geological and
- petrological implications. Petrology 24, 21-34.
- Niedermann, S., 2002. Cosmic-ray-produced noble gases in terrestrial rocks: dating tools for
- surface processes. Reviews in Mineralogy and Geochemistry. 47, 731-784.

- 592 Pritchard, C. J., Gaylord, D. R., Adams, D. B., Ernst, S., Hermanson, M., 2020. Role of
- 593 Quaternary glacial-outburst megaflood paleochannel deposits in a basalt-dominated aquifer
- system in the West Plains area of eastern Washington, USA. Hydrogeology Journal 28, 921-939.
- Protin, M., Blard, P., Marrocchi, Y., Mathon, F., 2016. Irreversible adsorption of atmospheric
- 596 helium on olivine: A lobster pot analogy. Geochimica et Cosmochimica Acta 179, 76-88.
- Reidel, S. P., 2005. A lava flow without a source: The Cohassett flow and its compositional
- 598 components, Sentinel Bluffs Member, Columbia River Basalt Group. The Journal of Geology
- 599 113, 1-21.
- Reidel, S. P., Camp, V. E., Tolan, T. L., Martin, B. S., 2013. The Columbia River flood basalt
- province: Stratigraphy, areal extent, volume, and physical volcanology. The Columbia River
- Flood Basalt Province: Geological Society of America Special Paper. 497, 1-43.
- 603 Schiffer, M., Stolz, A., López, D. A., Spanier, R., Herb, S., Müller-Gatermann, C., Heinze, S.,
- Binnie, S., Melchert, J., Kivel, N., 2020. Method developments for accelerator mass
- spectrometry at CologneAMS, ⁵³Mn/³He burial dating and ultra-small ¹⁴CO₂ samples. Global and
- 606 Planetary Change. 184, 103053.
- Shuster, D. L., Farley, K. A., Vasconcelos, P. M., Balco, G., Monteiro, H. S., Waltenberg, K.,
- Stone, J. O., 2012. Cosmogenic 3He in hematite and goethite from Brazilian "canga" duricrust
- demonstrates the extreme stability of these surfaces. Earth and Planetary Science Letters 329, 41-
- 610 50.

- Stone, J. O., 2000. Air pressure and cosmogenic isotope production. Journal of Geophysical
- 612 Research 105, 23753-23759.
- Stone, J., Evans, J. M., Fifield, L. K., Allan, G. L., Cresswell, R. G., 1998. Cosmogenic chlorine-
- 36 production in calcite by muons. Geochimica et Cosmochimica Acta 62, 433-454.
- 615 Swanson, D. A. and Wright, T. L., 1978. Bedrock geology of the northern Columbia Plateau and
- adjacent areas. in The Channeled Scabland: A guide to the geomorphology of the Columbia
- Basin, Washington, Baker, V. R. and Nummedal, D. eds. ch. 3, p. 37-57.







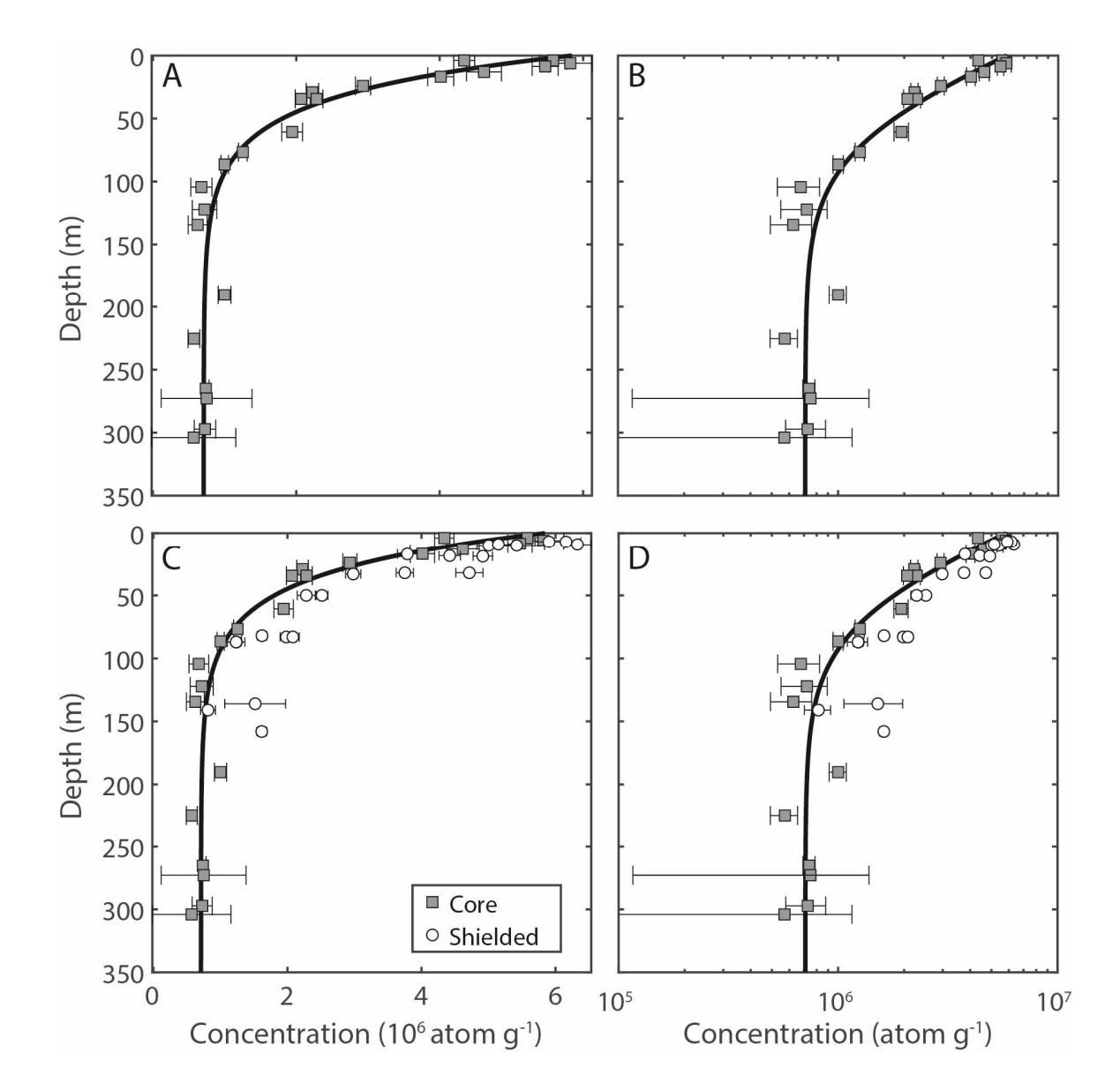


Figure 2. 3 He concentration versus depth. A and B) 3 He concentration versus depth for Cheney core samples plotted on linear and semi-log axes. C and D) 3 He concentration versus depth for the Cheney core and other samples shielded from spallogenic 3 He production. Error bars indicate 1 standard deviation (1 σ) uncertainties. The black curve shows the fit of equation (2) to the data from the core. Core samples from depths >87 m were used to define the nucleogenic 3 He concentration; samples from depths <87 m were used to determine the e-folding length and surface concentration of muon-produced 3 He.

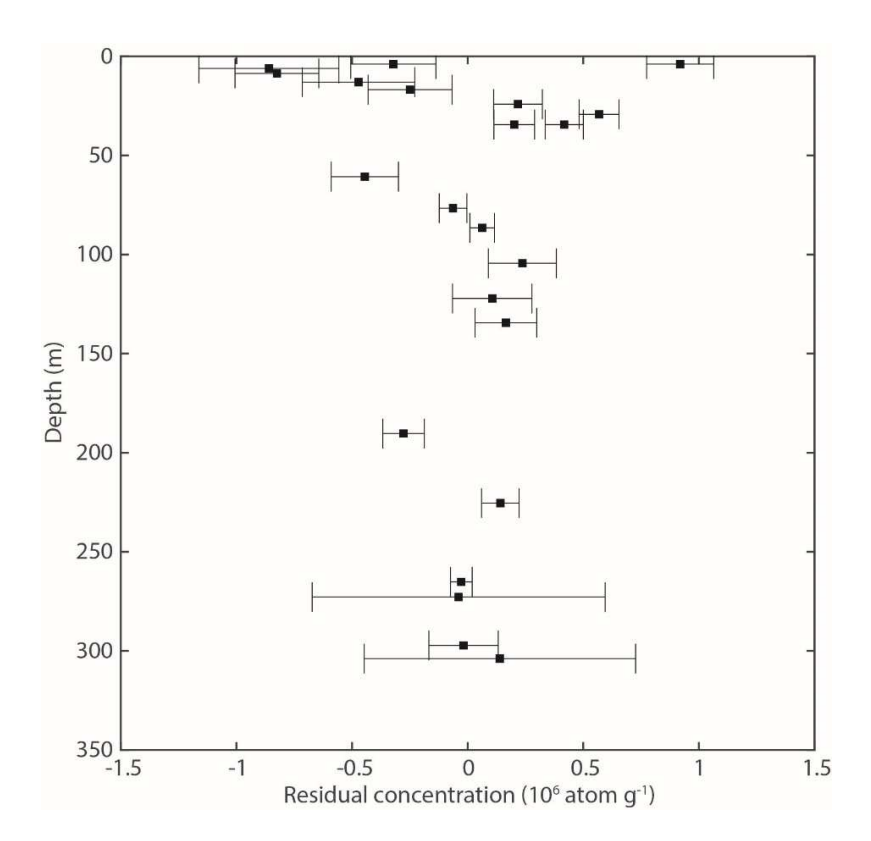


Figure 3. Residual 3 He concentrations. Values are measured concentrations subtracted from predictions based on the best fit of equation (2) to the Cheney core data. Error bars indicate 1σ uncertainties.

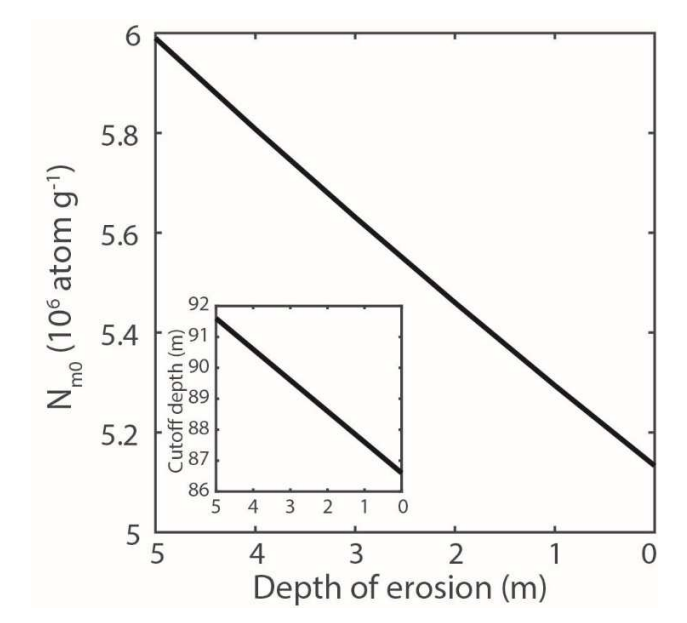


Figure 4. Sensitivity of surface muon concentration (N_{m0}) to instantaneous erosion of the basalt surface. The curve shows how recent, instantaneous erosion of the basalt surface of depths up to 5 m would alter the predicted surface concentration. The inset shows how instantaneous erosion would influence the cutoff depth, the depth below which muonogenic 3 He production is negligible compared to nucleogenic production.

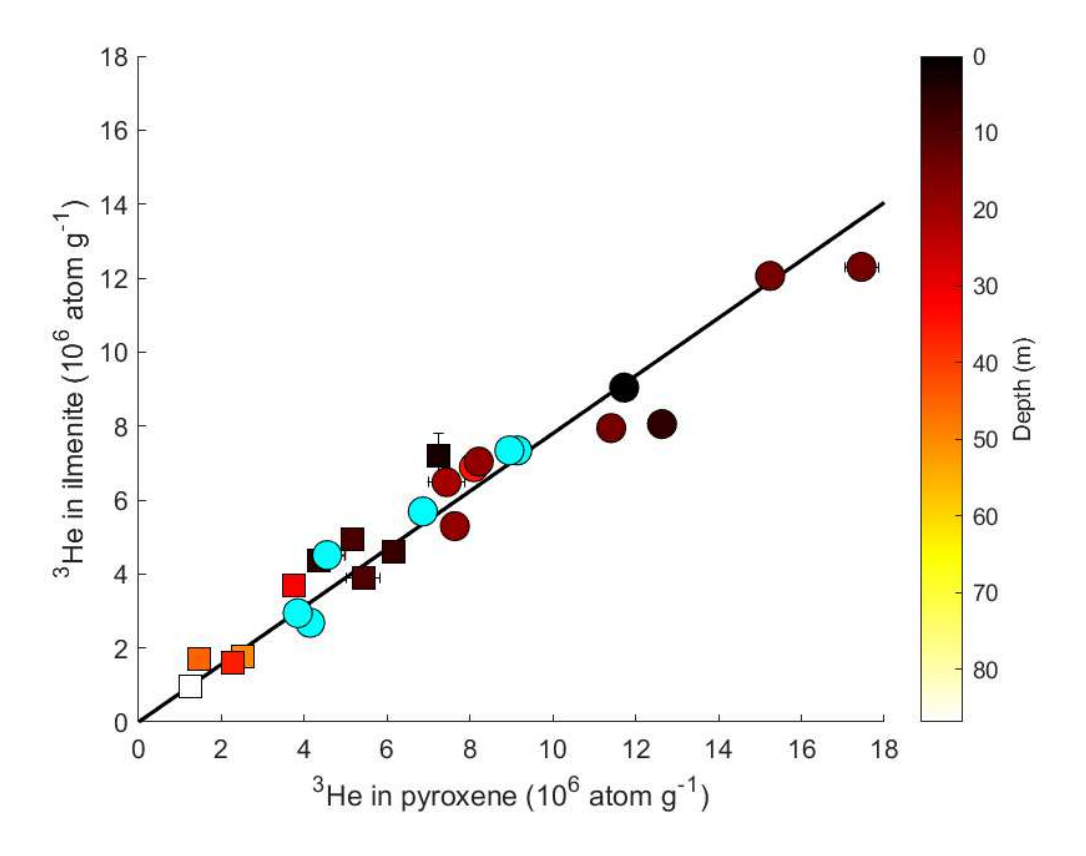


Figure 5. The ³He concentration in ilmenite versus pyroxene for samples shielded from spallogenic ³He production and un-shielded samples. Squares indicate measurements for Cheney core and shielded samples analyzed for this study. Circles indicate measurements from non-shielded bedrock and boulder samples from Larsen et al. (2019). The depth of bedrock samples below the inferred Miocene surface of the Columbia River Basalt is shown by the color bar. Samples from flood-transported boulders, where the sample depth is unknown, are shown as light blue circles. Error bars indicate 1σ uncertainties, which are generally smaller than the symbol size. (For interpretation of the colors in the figure, the reader is referred to the web version of this article.)

Table 1. Cheney core helium isotope abundance and sample depth data.

Sample ID	Mass	³ He	³ He 1σ SD	⁴ He	⁴ He 1σ SD	³ He/ ⁴ He	³He/⁴He 1σ SD	Depth	³ He pyroxene equivalent	³ He 1σ SD pyroxene equivalent
				(10 ¹² at g ⁻¹)		(R _A)	(R_A)	(m)	(10 ⁶ at g ⁻¹)	(10^6 at g^{-1})
Ilmenite		· · · · · ·	· · · · · · ·	<u> </u>	<u> </u>				<u> </u>	<u> </u>
*CRB1IL	0.1451	4.35	0.15	36.3	0.4	0.086	0.0030	3.9	5.58	0.18
CRB2IL	0.1466	4.54	0.28	53.2	2.7	0.061	0.0049	6.1	5.82	0.30
CRB3IL	0.1488	4.27	0.14	52.6	0.5	0.058	0.0020	8.6	5.47	0.18
CRB4IL	0.1490	3.60	0.22	59.6	3.0	0.043	0.0035	13	4.62	0.24
CRB5IL	0.0579	3.13	0.16	147.9	1.7	0.015	0.0008	16.8	4.01	0.18
CRB6IL	0.1550	2.29	0.01	92.4	0.9	0.018	0.0007	24.1	2.93	0.11
CRB7IL	0.1549	1.74	0.07	65.9	0.7	0.019	0.0008	29.2	2.23	0.09
CRB8IL	0.1565	1.61	0.07	40.9	0.4	0.028	0.0013	34.4	2.07	0.08
*CRB9IL	0.1566	1.70	0.20	28.7	2.9	0.042	0.0065	43.2	2.18	0.20
CRB10IL	0.1612	1.52	0.14	81.2	6.1	0.013	0.0016	60.7	1.94	0.15
0										
Pyroxene *CDD4D	0.4655	4.24	0.44	44.6	0.4	0.267	0.0002	2.0		
*CRB1Px	0.1655	4.34	0.14	11.6	0.1	0.267	0.0093	3.9		
CRB8Px	0.1548	2.28	0.09	3.8	0.04	0.426	0.0170	34.4		
*CRB9PX	0.0461	1.47	0.16	2.9	0.03	0.356	0.0382	43.2		
CRB12Px	0.1655	1.26	0.06	31.1	0.3	0.029	0.0014	76.6		
CRB13Px	0.1720	1.00	0.05	10.5	0.1	0.068	0.0037	86.5		
CRB14PX	0.0483	0.68	0.15	8.1	0.3	0.060	0.0133	104.4		
CRB15PX	0.0389	0.72 0.63	0.17	5.1	0.1 0.2	0.101 0.031	0.0241 0.0066	122.2		
CRB16PX CRB18PX	0.0513 0.1025	1.00	0.13 0.09	14.3 23.9	1.0	0.031	0.0000			
CRB18PX CRB21PX	0.1025	0.57	0.09	31.3	0.3	0.030	0.0029			
CRB21PX CRB22Px	0.0871	0.57	0.08	25.1	0.3	0.013	0.0019			
CRB23PX	0.1801	0.74	0.03	15.6	0.3	0.021	0.0013			
CRB23PX CRB24PX	0.0103	0.73	0.63	87.1	1.2	0.034	0.0291			
CRB25PX	0.0436	0.73	0.15	18.3	0.2	0.000	0.0012			
CNDZJFA	0.0111	0.57	0.39	10.3	0.2	0.022		303.9		

at = atom; SD = standard deviation; R_A = normalized to the atmospheric ratio of 1.39x10⁻⁶

^{*}Sample excluded from production rate and e-folding length calculation because the ilmenite to pyroxene ³He ratio is higher than expected value of 0.78±0.02 (Larsen et al., 2019)

Depth is relative to the top of the basalt exposed in the core. The drilling log indicates the basalt was overlain by 1.8 m of soil and gravel.

The location of the core is 47.478286 N and -117.59625 W (WGS 84) and the ground surface elevation is 719.3 m.